POLITECNICO DI TORINO
Repository ISTITUZIONALE

Modeling and On-Road Testing of an Electric Two-Wheeler towards Range Prediction and BMS Integration

Original
Modeling and On-Road Testing of an Electric Two-Wheeler towards Range Prediction and BMS Integration / Falai, Alessandro; Giuliacci, TIZIANO ALBERTO; Misul, DANIELA ANNA; Paolieri, Giacomo; Anselma, PIER GIUSEPPE. - In: ENERGIES. - ISSN 1996-1073. - ELETTRONICO. - 15:7(2022), p. 2431. [10.3390/en15072431]

Availability:
This version is available at: 11583/2960428 since: 2022-04-19T14:57:11Z

Publisher:
MDPI

Published
DOI:10.3390/en15072431

Terms of use:

This article is made available under terms and conditions as specified in the corresponding bibliographic description in the repository

Publisher copyright

(Article begins on next page)

02 September 2025

energies

MDPI

Article

Modeling and On-Road Testing of an Electric Two-Wheeler towards Range Prediction and BMS Integration

Alessandro Falai [1,2,*], Tiziano Alberto Giuliacci [1,3,*], Daniela Misul [1,2], Giacomo Paolieri [4] and Pier Giuseppe Anselma [2,5]

1 Department of Energy, Politecnico di Torino, Corso Duca Degli Abruzzi 24, 10129 Turin, Italy; daniela.misul@polito.it
2 Interdepartmental Center for Automotive Research and Sustainable Mobility (CARS@PoliTO), Politecnico di Torino, Corso Duca Degli Abruzzi 24, 10129 Turin, Italy; pier.anselma@polito.it
3 Addfor Automotive S.p.A., Piazza Solferino 7, 10121 Turin, Italy
4 Danisi Engineering, Via Ippolito Nievo 62, 10042 Nichelino (To), Italy; giacomo.paolieri@danisieng.com
5 Department of Mechanical and Aerospace Engineering, Politecnico di Torino, Corso Duca Degli Abruzzi 24, 10129 Turin, Italy
* Correspondence: alessandro.falai@polito.it (A.F.); tiziano.giuliacci@polito.it (T.A.G.)

Abstract: The automotive sector is currently shifting its focus from traditional fossil fuels to electrification. The deployment of a Battery Management System (BMS) unit is the key point to oversee the battery state of the electric vehicle (EV) to ensure safety and performances. The development and assessment of electric vehicle models in turn lays the groundwork of the BMS design as it provides a quick and cheap solution to test battery optimal control logics in a Software-in-the-Loop environment. Despite the various contribution to the literature in battery and vehicle modeling, electric scooters are mostly disregarded together with a reliable estimation of their performance and electric range. The present paper hence aims at filling the gap of knowledge through the development of a numerical model for considering a two-wheeler. The latter model relies on the conservation energy based-longitudinal dynamic approach and is coupled to a Li-Ion Battery second-order RC equivalent circuit model for the electric range prediction. More specifically, the presented work assesses the performance and electric range of a two-wheeler pure electric scooter in a real-world driving cycle. The e-powertrain system embeds an Electrical Energy Storage System (EESS) Li-Ion Battery pack. On-road tests were initially conducted to retrieve the main model parameters and to perform its validation. A global battery-to-wheels efficiency was also calibrated to account for the percentual amount of available net power for the vehicle onset. The model proved to properly match the experimental data in terms of total distance traveled over a validation driving mission.

Keywords: electromobility; efficiency; electric two-wheeler; lithium-ion battery; numerical modeling; range prediction; real-world testing

check for updates

Citation: Falai, A.; Giuliacci, T.A.; Misul, D.; Paolieri, G.; Anselma, P.G. Modeling and On-Road Testing of an Electric Two-Wheeler towards Range Prediction and BMS Integration. *Energies* **2022**, *15*, 2431. https://doi.org/10.3390/en15072431

Academic Editor: Fabrice Locment

Received: 25 February 2022
Accepted: 22 March 2022
Published: 25 March 2022

Publisher's Note: MDPI stays neutral with regard to jurisdictional claims in published maps and institutional affiliations.

Copyright: © 2022 by the authors. Licensee MDPI, Basel, Switzerland. This article is an open access article distributed under the terms and conditions of the Creative Commons Attribution (CC BY) license (https://creativecommons.org/licenses/by/4.0/).

1. Introduction

In the recent years, electric mobility has become increasingly popular due to its high potential for significant reductions in pollutant emissions and greenhouse gases. As an example, the electric vehicle sales summed up to more than 400,000 units in 2020 and grew exponentially by 157% during the last year [1]. Such figures mark a fundamental turning point in the market trend of electric vehicles. It is anyhow worth recalling that one of the most important components for e-powertrains is the Electrical Energy Storage System (EESS), which is the key energy source for e-mobility applications [2].

Still, several limitations oppose to the global diffusion of electric vehicles. On the one hand, the e-vehicle autonomy is likely to range at low values, from 100 to 300 km only [3], and is to be ascribed to the battery sizing. Still, the higher the battery pack capacity, the higher the costs, the vehicle load and, consequently, the energy consumption. Hence, specific attention should be driven to identifying a proper trade-off needs between

electric range and battery size. A fundamental advantage of e-powertrains relates to the higher efficiency of the electric motors at low vehicle speed with respect to internal combustion engines (ICEs). As a result, urban areas are the primary targets for electric mobility. Still, considering the sparse and rare distribution of electric charging stations [4] together with the lack of widespread fast charging infrastructure [5], range anxiety should be properly addressed and overseen by accurate predictive models. Finally, considering that two-wheelers have always represented a compelling solution for urban traffic, electric two-wheelers are prone to represent a major milestone in electric mobility. A detailed vehicle model describing the dynamic behavior is provided in [6] to improve the design and manufacturing ability of electric scooters.

On the other hand, electric two-wheelers require the development of dedicated battery management systems (BMS) to ensure suitable performance and electric range. Still, the BMS deployment and implementation in turn requires a deep knowledge of the vehicle as well as of the battery behaviors. As far as the battery is concerned, the use of lithium is now widely spread. Lithium-ion batteries (LIBs) are characterized by complex yet effective electrochemical operations and exhibit high stored energy, high-power density, long life, low self-discharge, low maintenance costs and low environmental impact. Hence, the study of LIBs together with their modeling are key issues for the analysis of performance and application limits as well as for the development of a customized, flexible, and reliable BMS [7,8].

LIB performance models are classified into three main families: electrical models [9,10], analytical models [11,12] and electrochemical models [13,14]. The levels of accuracy and the degree of complexity inversely decreases in support of computational cost saving. Amongst the electrical models, the equivalent circuit models (ECM) [15] proved to be suitably employed in a system-level perspective for investigating into the BMS controllers [16] thanks to its high accuracy and low computational cost. The present work relies on the Thevenin equivalent circuit description: Each battery cell is described by a second-order equivalent circuit model through a combination of resistors, capacitances and voltage source. Issues related to the battery thermal management are widely investigated in the literature [17,18] but were not considered for the present research paper.

The previously mentioned models are widely used to characterize LIBs on most car segments as well as light-duty and heavy-duty vehicles [19]. However, as far as electric two-wheelers are concerned, the literature lacks applications of the Li-ion battery pack model as embedded in a system-level model and major gaps arise for the battery dynamic characterization and validation through on-road experimental tests.

In order to contribute filling the highlighted chasm of knowledge, the present paper aims at developing a numerical model of an electric two-wheeler for performance and range prediction. The developed numerical model is validated by means of experimental measurements collected during on-road tests of a prototype electric two-wheeler. The model is embedded in a Software-In-the-Loop environment and lays the groundwork for the BMS development. Several strategies and control logics could be tested in future works for the battery optimal management. Moreover, the deployed tool will be helpful to analyze and compare different battery architectures and configurations.

2. Materials and Methods

In this work, several experimental tests are carried out on a prototype electric two-wheeler. The on-road tests were conducted in Turin (Italy). In order to assess the vehicle behavior in terms of energy consumption, a physical-based model has been developed, and afterwards, it was coupled with a battery model. The model identification and validation were performed using the experimental data collected in several road tests.

The battery pack is a prototype consisting of 180 cells in 20s9p configuration. Each of the 9 modules in parallel is composed by SAMSUNG INR21700-50E cells. Cell dimensions are reported in Figure 1, while technical specifications are listed in Table 1. As concerns the battery pack, the related technical information is reported below in Table 2.

Table 1. Technical specifications of SAMSUNG INR21700-50E cell as reported on Samsung company datasheet [20].

Parameters	Values	Measurement Unit
Cell Format	Cylindrical	-
Technology	Li-Ion	-
Nominal Voltage	3.6	V
Nominal Capacity	4.9	Ah
Maximum continuous discharge current	9.8	A
Maximum non continuous discharge current	14.7	A
Recharge maximum current	4.9	A
Discharge Cut-off Voltage	2.5	V

Table 2. Technical specification of the prototype battery pack.

Parameters	Values	Measurement Unit
Pack configuration	20s9p	-
Nominal Voltage	72	V
Nominal Capacity	44.1	Ah
Total Energy	3.17	kWh
Maximum continuous discharge current	88.2	A
Maximum non continuous discharge current	117.6	A
weight	12.5	kg

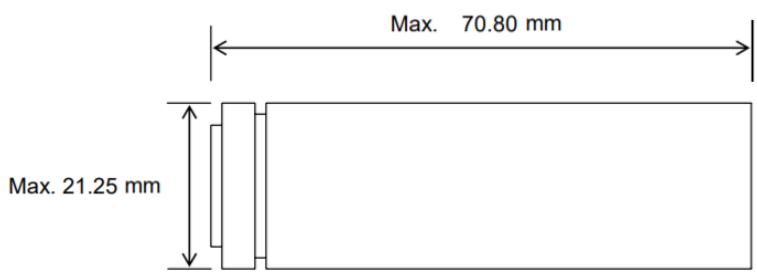

Figure 1. Outline dimensions of INR21700-50E.

2.1. Modeling Approach

In this activity, the implemented modeling method relies on an energy-based approach, which considers the electrical energy provided by the battery flowing through the vehicle drivetrain components to the driven wheels.Each considered drivetrain component can be modeled as described in the following sections. The software used for the data post-processing and model-building were Matlab© and Simulink©. The most useful toolboxes for this purpose were DSP System and the Model Identification [21]. The physical differential equations are solved through Simulink and the general vehicle modeling work is organized in two blocks: The battery modeling and the vehicle chassis modeling, as it can be seen in the global model overview shown in Figure 2. The battery model takes the driver current request as input, which may be also calculated using the opening of the accelerating knob, and returns the output battery pack electrical power. Then, the battery pack electrical power is delivered to the vehicle model in order to estimate the vehicle longitudinal speed. From the global view point, the global model receives battery current as input and predicts the actual two-wheeler longitudinal speed.

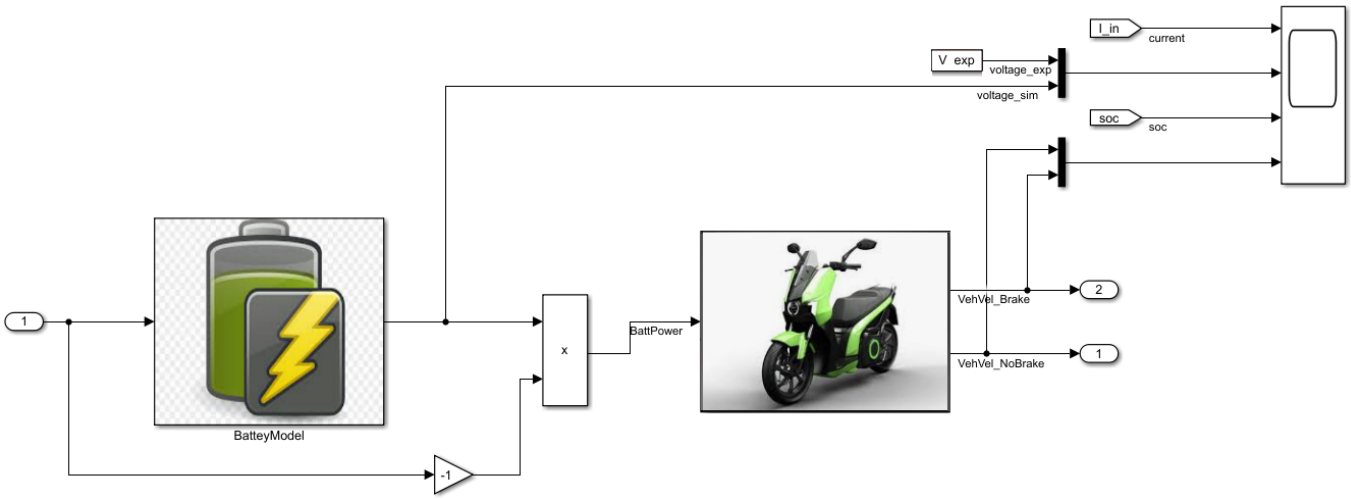

Figure 2. Global model implemented on Simulink. It includes the battery model connected to the the dynamic vehicle model.

2.1.1. Battery Model

There are several techniques available in the literature for lithium-ion battery modeling based on different levels of detail A second-order Equivalent Circuit Model (ECM) [22] is widely employed in several applications [7,23,24] in order to capture both fast dynamic events, e.g., resistance and charge transfer effect, and slow dynamic events, e.g., diffusion effects. In the present work, the ECM was exploited to characterize each single cell as they are smaller energy storage systems and the base unit of the battery pack. The behavior of each cell can be analyzed independently, which lays the groundwork for the development of BMS control logics.

In Figure 3, V and I are, respectively, the cell terminal voltage and current, V_j with $j = 0, 1, 2$ are voltage drops across resistors based on flowing current. R_0 and R_j and C_j with $j = 1, 2$ are the time-varying model parameters corresponding to resistors and capacitors which model both the static and dynamic behaviors of the cell. Specifically, R_0 determines the cell static resistance, and each RC pair determines a different time constant dynamic behavior: the first R_1C_1 models charger transfers and the double layer effect, while the last pair of R_2C_2 are employed to catch the cell diffusion effects occurring at a much higher time scale. The OCV is the cell Open-Circuit Voltage, which is modeled as an ideal voltage source. All these parameters depend on the cell's State Of Charge (SOC).

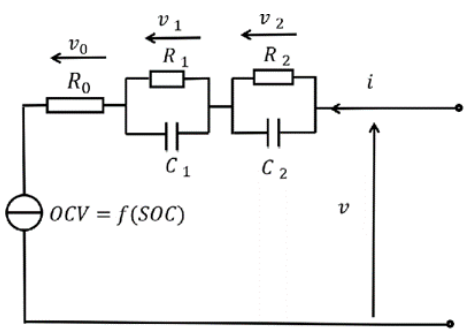

Figure 3. The Equivalent Circuit Model of lithium-ion battery with all model parameters which describe the operation of a single cell.

In some advanced modeling approaches, hysteresis for the OCV [25] and parasite current phenomena are included. These two aspects were not considered in this work in order to preserve the simplicity of the model while obtaining a satisfactory accuracy.

As previously indicated, the number of RC pairs is directly linked to the model order, which is a trade-off between model accuracy and complexity. For Li-ion batteries, an ECM with two RC networks is commonly employed and it achieves a good level of accuracy [26].

The time-continuous cell model is described by the ECM according to the the following equations:

$$\begin{cases} \dfrac{dV_1}{dt} = -\dfrac{V_1}{R_1C_1} + \dfrac{I}{C_1} \\ \dfrac{dV_2}{dt} = -\dfrac{V_2}{R_2C_2} + \dfrac{I}{C_2} \\ \dfrac{\mathrm{SOC}}{dt} = -\dfrac{I}{Q_{cell}} \end{cases} \tag{1}$$

where Q_{cell} is the cell nominal capacity in ampere-seconds. The only variable in (1) is the current amplitude I. Once all parameters have been defined, the model takes the current I as input and solves a first-order differential equation which is able to simulate the total voltage delivered by the cell according to the Second Kirchhoff's Law:

$$v = \mathrm{OCV} - R_0 I - V_1 - V_2 \tag{2}$$

This modeling approach was implemented in a Simulink block, and it forms the first part of the global vehicle model: For a current input, it returns an output voltage value. The single cell model was exploited in order to create the general battery pack model by connecting several cell models according to the battery pack configuration, which is 20s9p. The 20 ECMs were connected in series to create a single module, and then 9 modules were connected in parallel to reproduce the pack, as schematized in Figure 4.

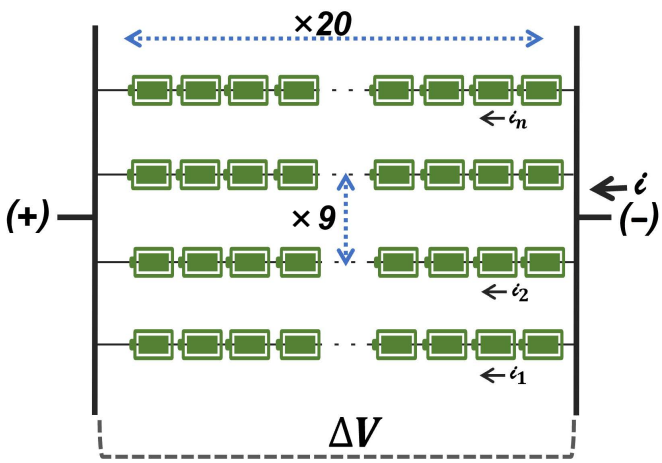

Figure 4. Battery pack modeling: 9 modules are connected in parallel and each module has 20 cells connected in series, each single one modeled as an independent ECM: 'i' is the battery pack current, and ΔV is the voltage of the battery pack.

The Simulink implementation was performed by exploiting the Simscape Electrical libraries: The entire battery pack model is illustrated in Figure 5. The first layer of the Battery Pack model composed by 9 modules in pair is represented inside the black box; each of the 9 modules are composed by 20 cells connected in series (green box). In the red box, a single-cell structure is reported: an SOC block estimation is present, too, and it is useful to evaluate the parameters in the Look Up Table. This allows each cell to have a different behavior. According to the Simulink libraries, the blue lines represent electrical connections, the red lines the physical connections and the black ones the signals connections.

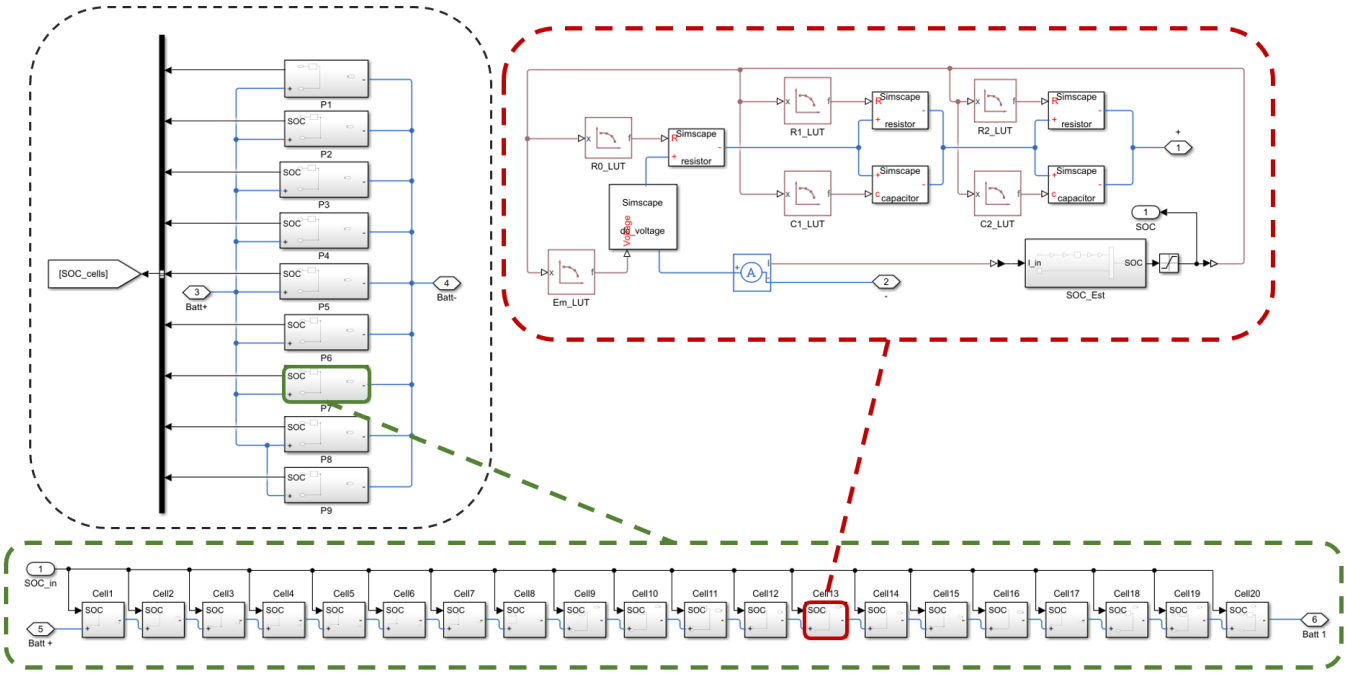

Figure 5. Model of the battery pack configuration on Simulink virtual environment.

As already discussed for Figure 3, each cell was modeled as a *2RC-ECM*, and the unknown parameters which characterize the cell model properties are:

- OCV [V];
- R_1 [Ω];
- C_1 [F];
- R_0 [Ω];
- R_2 [Ω];
- C_2 [F].

These are implemented in appropriately calibrated one-dimensional look-up tables as a function of SOC. The SOC for each cell is in turn evaluated according to the Coulomb Counting equation. This is obtained by integrating the third equation of (1) as follows:

$$\mathrm{SOC}_t = \mathrm{SOC}_{T0} - \int_{T0}^{t} \frac{I}{Q_{cell}} dt \tag{3}$$

This approach enables the modeling independence of each cell, and this is necessary for future BMS integration and the development of some future optimization strategies, such as cell equalization, for example. However, this makes the model more expensive from the computational load point of view. In this phase of the activity, all the cells were modeled assuming the same values for all the parameters, which makes them identical. This assumption is a good approximation of the reality considering that the cells in the tested battery pack are new and they should therefore be identical [27], assuming appropriate manufacturing tolerances [28,29]. After the present work, a dispersion regarding values of the parameters will be investigated in order to analyze the battery pack behavior more realistically.

2.1.2. Longitudinal Dynamic Model

The physical modeling of the longitudinal vehicle dynamics can be defined by considering the general equation of the instantaneous energy balance for the two-wheeler's body:

$$m_{tot}\, a\, v = P_{mot} - P_{diss}, \tag{4}$$

where m_{tot} is the vehicle equivalent mass; v and a are the velocity and the acceleration, respectively, of the two-wheeler's center of gravity at a specific time instant t; P_{mot} is the power generated by the electrical motor; and P_{diss} stands for the power of all the dissipative phenomena occurring. By integrating Equation (4) over a time interval, the energy associated to the body can be calculated as follows:

$$\int m_{tot}\, a\, v\, dt = \frac{1}{2}\, m_{tot}\, v^2 \tag{5}$$

The total energy of the vehicle body is related to two contributions: the longitudinal speed and the rotational speed of the drivetrain components. Among the latter, the most important one is the rotatory inertia of the electric motor, which absorbs part of the traction power delivered by the battery, and it dissipates power in deceleration phases. The same holds for the mechanical transmission, yet its contribution can be assumed as negligible. Hence, just the inertia of the electric motor was considered in this work. Equation (4) can thus be written as follows:

$$m_{tot}\, a\, v = m\, a\, v + J_{motor}\, \theta\, \dot{\theta}. \tag{6}$$

Considering Equation (6), m is the translating mass of the vehicle, consisting of the sum of vehicle and driver masses; J_{motor} is the motor rotating inertia, while θ and $\dot{\theta}$ are the motor rotational velocity and its acceleration, respectively. By considering the vehicle transmission kinematics, we obtain the following equation:

$$J_{motor} \cdot \theta \cdot \dot{\theta} = J_{motor} \cdot \frac{\tau^2}{R^2} \cdot v \cdot a. \tag{7}$$

where R is the wheel dynamic radius, and τ is the speed ratio between the motor and the driven wheel rotational velocity. Two-wheelers equipped with internal combustion engine (ICE) generally embed a CVT (continuously variable transmission). However, nowadays, CVTs are solutions generally not exploited for electric vehicles [30]. The drivetrain of a two-wheeler is an "in-body" transmission. Hence, it is reasonable to assume τ as a constant parameter. So, it can be assumed:

$$J_{motor} \cdot \frac{\tau^2}{R^2} = m_r; \tag{8}$$

Therefore, the left-side term of Equation (4) becomes:

$$m_{tot}\, a\, v = (m + m_r)\, a\, v \tag{9}$$

where m_{tot} is the equivalent mass.

As far as the motor power P_{mot} is concerned, it is considered corresponding to the battery power model output $P_{battery}$, V and I being the voltage and the current delivered by the overall battery pack, respectively, and assuming a battery-to-road efficiency η_{b2r} due to electrical and mechanical energy conversion (e.g., inverter, power electronics, bearings, tire friction and other transmission loss terms):

$$P_{mot} = \eta_{b2r}\, V\, I \tag{10}$$

As far as the dissipative terms are concerned, different contributions could be included into the equation term P_{diss} depending on the level of accuracy required. P_{diss} is equal to the product of the overall dissipative force acting on the vehicle F_{diss} times its velocity v:

$$P_{diss} = F_{diss}\, v. \tag{11}$$

In this discussion, the main phenomena considered in F_{diss} are:

- Aerodynamic forces: These represent the air resistance to motion and depend on the square of vehicle velocity, air proprieties and geometrical vehicle shape. The mathematical formulation is:

$$F_{Aerodynamic} = \frac{1}{2} \cdot \rho_{air} \cdot A_f \cdot C_x \cdot v^2, \tag{12}$$

more precisely, ρ_{air} is the air density, A_f is the frontal area of the vehicle and C_x is a dimensionless parameter lower than 1 called the Drag Coefficient, which describes the aerodynamics of the body. According to the mathematical formulation, the lower this coefficient's value, the better the aerodynamic performances of the considered vehicle.
- Tire Rolling Resistance: This represents the resistance produced by the contact between tires and the road surface. The energy dissipation of this term is due to the elastic micro-deformation in the tire body. Its magnitude is modeled by the following formula:

$$F_{Tire} = m \cdot g \cdot f \cdot cos(\alpha), \tag{13}$$

The α parameter indicates the road grade, g is the gravity acceleration and m is the vehicle mass. Particular importance is give to the value of the f coefficient, which is called the *rolling resistance coefficient*, and it depends on the tire composition and the road surface material. Concerning passenger cars, its value can range from 8 $\frac{\text{kg}}{\text{t}}$ considering homogeneous asphalt [31] and normal tires up to 45 $\frac{\text{kg}}{\text{t}}$ considering an off-road path [32]. The F_{Tire} formulation can also include a factor which depends on the square of vehicle velocity and an f_2 coefficient, but because this values is quite small, considering the application of a two-wheeler, these were neglected in this work.
- Gravity Resistance: this is the resistance force produced by the road slope. Its value can be calculated as:

$$F_{Slope} = m \cdot g \cdot sin(\alpha); \tag{14}$$

Since all the experimental tests were driven on approximately flat road, the values of both α and F_{slope} are considered, too.

All the other elements which cause the dissipation of energy and which are not included above (for instance, the internal friction between the mechanical elements) will be afterwards considered in a generic factor standing for the overall efficiency of the system. In general, the sum of the dissipative forces F_{diss} can thus be broken down according to the following equation:

$$F_{diss}(v) = F_{Aerodynamic} + F_{Tire} + F_{Slope} = \frac{1}{2}\rho_{air} A_f C_x v^2 + mgfcos(\alpha) + mgsin(\alpha) \tag{15}$$

which is rewritten in the following form:

$$F_{diss} = A + B \cdot v + C \cdot v^2, \tag{16}$$

with:

$$\begin{cases} A = mgf; \\ B = 0; \\ C = \frac{1}{2}\rho_{air} A_f C_x; \end{cases} \tag{17}$$

Finally, the vehicle velocity can be obtained from the battery electrical power solving Equation (4), which is re-organized as follows:

$$\left(m + m_r\right) v \frac{dv}{dt} = \eta_{b2r} \cdot VI - v\left(A + Cv^2\right). \tag{18}$$

where the acceleration a is written as $\frac{dv}{dt}$ exploiting the differential relationship.

Equation (18) is implemented in the second block (shown in Figure 6) of the global model, and it can estimate the final vehicle kinematics, with particular interest in the longitudinal velocity profile over time. The input of this block is the battery electrical power.

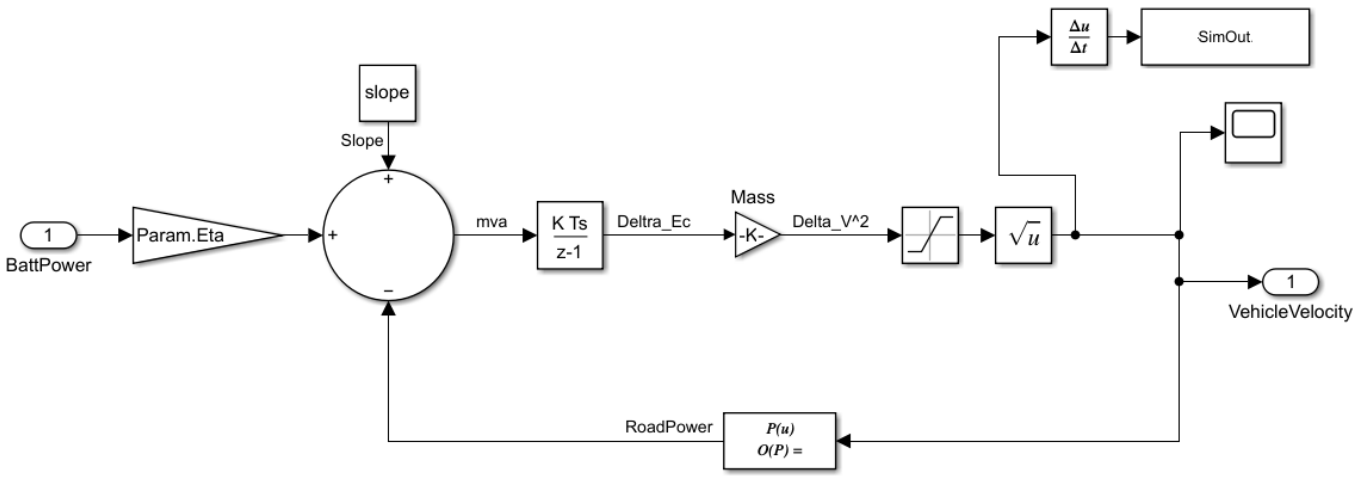

Figure 6. Longitudinal dynamics of two-wheeler block using through a physical-based energy approach on Simulink.

2.2. Test and Data Acquisition

Data were acquired for the prototype two-wheeler over different driving missions. This was performed by equipping the two-wheeler with an acquisition board able to record signals from vehicle standard sensors used for the internal communication between the ECU (Electronic Control Unit), the BMS (Battery Management System) and the driver monitor and send them on a CANbus to an external data logger. The data acquisition was handled by the commercial software DEWEsoft® on a user device and finally memorized on a dedicated memory. No other external devices were integrated except an analog Hall's effect current (LEM) sensor which improves the quality of the signals acquired: Indeed, this sensor has higher reliability, accuracy and sampling frequency. The main signals of interest collected through the BMS channel were the total voltage and current delivered by the battery pack, the lower and the higher values of temperature and the voltage concerning the internal battery cells. Moreover, the State of Charge (SOC) and the State of Health (SOH) computed by the vehicle BMS were collected as well. On a separate channel, the opening of the throttle knob in terms of percentage and the vehicle speed were collected as analog signals.

Several test sessions were performed aiming at defining the unknown parameters inside the battery model and the longitudinal-dynamic vehicle model. Different tests were performed and listed in Table 3.

Table 3. Test Session dataset available for the model identification

Test	Test Type/Session	Test Specifications	Repetitions
1	Discharge	SOC in range [1, 0.3]	1
2.1	Coastdown 1	(from 22 to 8) m/s	4
3.1	Coastdown 2	(from 22 to 8) m/s	4
3.2	Coastdown 2	(from 22 to 8) m/s	4
4.1	Coastdown 3	(from 22 to 8) m/s	4
4.2	Coastdown 3	(from 22 to 8) m/s	4
5.1	Constant Speed 1	5.5 m/s	2
5.2	Constant Speed 1	11 m/s	2
5.3	Constant Speed 1	16.5 m/s	2
5.4	Constant Speed 1	22 m/s	2
6.1	Constant Speed 2	5.5 m/s	2
6.2	Constant Speed 2	11 m/s	2
6.3	Constant Speed 2	16.5 m/s	2
6.4	Constant Speed 2	22 m/s	2
7	Partial Knob	50%	1

The selected route for test #1 is shown in Figure 7, while the route for the remaining tests is shown in Figure 8. The same 'Test Type/Session' name refers to different tests performed in the same operating conditions. More details about tests conditions are provided below.

Figure 7. Selected route in Turin, Italy, for performing on-road tests for the prototype two-wheeler. The route is driven to calibrate the battery model.

Figure 8. Selected route in Turin, Italy, forperforming on-road tests for the prototype two-wheeler. The route is driven to calibrate the dynamic vehicle model.

As far as the battery characterization tests are concerned, a driving mission was steadily repeated until the vehicle shut down due to battery voltage cut-off by the BMS. This included accelerating, constant speed and braking phases. The battery installed on the vehicle is not the one associated to the on-board BMS but rather a prototype pack featuring an approximately 50% higher capacity compared with the one which the on-board BMS is intended for. When the on-board BMS detects that the capacity delivered by the battery is close to the limit imposed by the manufacturer (which is calibrated on the non-oversized production battery), it disables the vehicle and switches it off in order to prevent a potential situation of under-voltage. This setting could not be changed or modified, and therefore totally discharging the prototype battery pack while driving was not possible. Because of this, the prototype battery was discharged only for about 70% of its capacity, while no characterization was possible below this threshold. Moreover, in the acquisitions, no temperature data were available. Therefore, in this work the battery has been modeled in a portion of its SOC operating field, and the dependency on the temperature was not considered. The performance of the model thus refers only to the standard ambient condition in this work. The overall test for identifying the values of cell parameters in the numerical model by steadily repeating a real-world driving mission is shown in Figure 9.

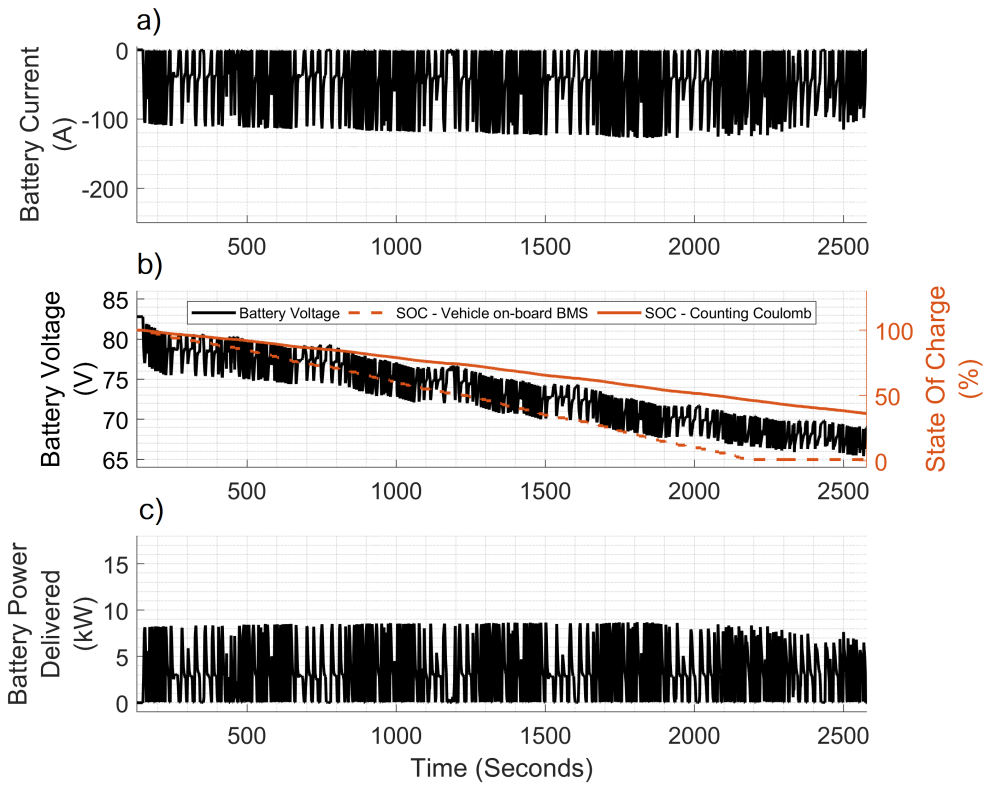

Figure 9. Test #1: (**a**) current (**b**) voltage and (**c**) power delivered by the battery during a drive mission for a discharging test session with the SOC estimation performed by the stock BMS of the electrical vehicle and by a post-processing of the data through the Counting Coulomb method.

The post-processing SOC estimation performed in this work exploits Equation (3). From the literature, it can be seen that several SOC estimation methodologies take into account the battery capacity: This may explain the reason why the original BMS of the two-wheeler performs a wrong SOC estimation when monitoring the prototype pack. However, for these analyses, it was considered only the post-processing estimated SOC as obtained by the Coulomb Counting. This method has a strong reliable computation once the initial condition SOC_{T0} is known [33,34], which is satisfactory for our current purposes.

As far as the dynamic model identification part is concerned, several test sessions were carried out in different locations in Turin (Italy). These were used to determine the coefficients of the equations modeling the friction and the global motor efficiency. In the test sessions, different types of specific drive missions were performed by the two-wheeler driver as it can be observed in Table 3:

- Coastdown: It consists in accelerating the vehicle until a certain speed and then letting the vehicle decelerate on an approximately flat road without braking and without significant wind conditions. Furthermore, during these tests, it is very important that no gear is engaged in order to verify the hypothesis of no torque being produced by the inertia of the rotating elements of the driveline applied on the wheel [35,36]. However, this could not be performed due to absence of a manual gear selector in the two-wheelers. In these tests, the two-wheeler started the coastdown phase from a speed of around 80 km/h (22.2 m/s). Many repetitions were recorded. An example coastdown test can be observed in Figure 10.
- Constant speed: The vehicle keeps the same velocity for many seconds several times. Four different speeds were considered: 20, 40, 60 and 80 km/h.
- Constant partial opening of the accelerating knob: The driver kept the opening of the accelerating knob constant for a few seconds.

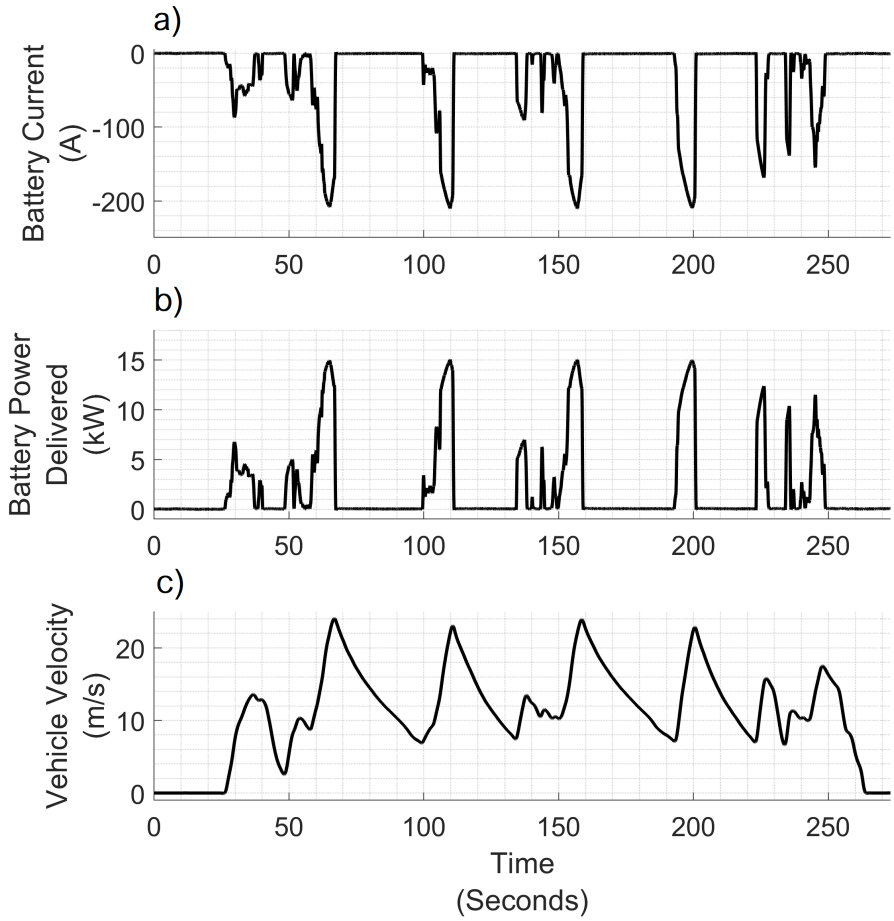

Figure 10. Test #3.1: (**a**) current and (**b**) power (kW) delivered from the battery and (**c**) vehicle velocity profile during a Coastdown test session composed by several acceleration and deceleration phases.

2.3. Data Processing

The acquired data were managed during the post-acquisition phase following a data handling procedure. Before being used for the model identification task, data logging coming from on-road test acquisitions were pre-processed with the aim to check their consistency, robustness and quality. Moreover, the presence of missing data, spikes, outliers or any other unwanted phenomena was examined. These, for instance, may be caused by a temporary malfunctioning in some sensors. This data-cleaning process is significantly relevant for ensuring robustness and reliable results. Some signals were filtered or resampled, too, if needed. Moreover, the synchronization between the various channel was verified. Therefore, the dataset was prepared to be used for the following analysis. In coastdown acquisitions, for instance, the decelerating phases (which allow to identify the coefficients of the resistance forces) were cut and isolated by the rest of the test and regrouped together. The same operation was conducted considering constant speed acquisitions.

2.4. Model Identification

In order to completely define the global model, the unknown parameters must be determined. These are estimated and validated using multi-experiment data according to the information resumed in Table 4. The parameter identification for the two numerical models (the battery model, and the vehicle dynamic model) was developed separately with a different dataset. The battery model was calibrated exploiting dataset #1, while the dynamic model exploited datasets #2.1, #3.1, #4.1 and #5. Both single models and the global model were tested on the same dataset group, composed by datasets #3.2, #4.2, #6 and #7.

Table 4. Used Datasets for model identification and testing, with reference to Table 3.

	Model Identification	Model Testing
Battery Model	1	3.2–4.2–6–7
Dynamic Vehicle Model	2.1–3.1–4.1–5	3.2–4.2–6–7
Global Model	-	3.2–4.2–6–7

2.4.1. Battery

The *Parameter Estimator* tool available in Simulink [37,38] and based on a Non-Linear Least Square (NLS) method optimization was used. This is based on the Region-Reflective-Trust algorithm [39,40], which is a widely used technique in the literature [41].

The model implementation was handled for each parameter through a 1D look-up table (LUT) as a function of the cell SOC. The domain of the LUT, i.e., the SOC values, was discretized in the range 0 to 1, with a 0.1 step. However, according to the modeling methodology explained in the previous paragraph, 6 LUTs with dimension of 10×1 each must be defined for each cell. The battery model being composed of 180 cells, the number of unknown parameters is quite large.

In order to simplify the optimization process and reduce the calculation time, the hypothesis of equality among the cells was exploited, reducing the problem into the determination of the parameters of just one representative cell. This was conducted by exploiting a simple Simulink model with just one cell and considering the cell current $\bar{I}_{cell}$, which can be obtained by dividing the total current I by the number of modules, nine in this case. An analog procedure was performed for the total voltage by considering the number of cells in series:

$$\begin{cases} \bar{I}_{cell} = \dfrac{I}{\text{number of modules}} \\ \bar{V}_{cell} = \dfrac{V}{\text{number of series}} \end{cases} \tag{19}$$

The optimization tool has a graphic user interface, where the NLS method was set for the objective function minimization definition and data were specified for the input and the output and the parameters to be identified. Afterward, the calibration process began, and the numerical values for the variables of interest were iteratively determined by evaluating and minimizing the error function between the model output voltage and experimental measured voltage.

2.4.2. Vehicle Longitudinal Dynamics

Dealing with the definition of the dynamic model part, the aim is to define the values of the constants A, C, η_{b2r} and m_r from Equation (18). In order to fulfill this task, the identification process was split into two phases characterized by a slightly different procedure.

The first phase aims at defaining only A and C (i.e., the coefficients of the dissipative forces), and it exploits the coastdown tests. This was performed because, in these tests, the action of the dissipative force is isolated and the terms η_{b2r} and m_r are not present. In the real-world the power delivered by the motor is zero; however, disengaging the motor by the wheel and removing the torque produced by the inertia of the rotating element is not possible. Because of this, the term m_r could not be removed, and an iterative procedure was therefore carried out. At the first moment, m_r was imposed equal to 0, and numerical values for the parameters A and C were identified. Knowing A and C and exploiting the entire coastdown maneuvers, plus the other test available at constant velocities, the parameters m_r and η_{b2r} were then identified. After that, the value obtained for m_r was used in order to restart the whole procedure. Several iterations were performed until the value obtained for m_r was strictly close to the value at the previous step.

For this task, too, the NLS (*non-linear least square*) method with the *Trust-Region-Reflective* algorithm implemented by MathWorks® in the Optimization Toolbox™ was exploited. However, in this case the optimization problem was not defined through the Parameter Identification Tool but it was manually defined by exploiting many Matlab functions. For the first part of the problem, the objective function to minimize is reported in Equation (20), which is obtained from Equation (18) while setting the motor power to 0:

$$min\{(m + m_r)v\frac{dv}{dt} + v\left(A + Cv^2\right)\}; \tag{20}$$

where the vehicle velocity v is the unique signal needed, and it is expressed in m/s according to the S.I. convention.

Once the coefficients A and C were defined, in order to identify m_r and η_{b2r} the following objective function was minimized in the second part of the problem:

$$min\{(m + m_r)v\frac{dv}{dt} + \eta_{b2r}\, V\, I + v\left(A + Cv^2\right)\}. \tag{21}$$

The two-wheeler is not able to recover energy during regenerative braking. Hence, the deceleration phases of driving missions are covered by mechanical brakes.

3. Results and Discussion

As stated before, a global model composed by Li-ion battery and vehicle body modeling is developed and tuned based on experimental tests carried out over real-world driving conditions. Hence, for the testing phase, the model prediction was compared with the experimental data, and the errors on the datasets were statistically investigated in order to analyze the quality of the regression; this was performed by considering the following metrics:

- The *Root-Mean-Square Error* (*RMSE*):

$$RMSE = \sqrt{\frac{\sum_{i=1}^{n} x_i - \hat{x}_i{}^2}{n}} \tag{22}$$

- The determination coefficient, *R squared* (R^2):

$$R^2 = 1 - \frac{\sum_{i=1}^{n}(x_i - \hat{x}_i)^2}{\sum_{i=1}^{n}(x_i - \bar{x}_i)^2} \tag{23}$$

where x_i is the experimental measured data, $\hat{x}_i$ is the model estimated value, $\bar{x}_i$ is the mean of experimental measured data in the considered test session and n is dataset sample size.

The main physical values used for the performance evaluation are the battery power and voltage, the vehicle velocity, the distance traveled and the electrical energy delivered in the whole test. Initially, the battery model and vehicle model results are shown and analyzed separately. Then, the global model performance is investigated and benchmarked in order to compare the distance experimentally covered by the vehicle and the one predicted by models. This parameter is taken as main metric in the model evaluation when the aim is range estimation. Thus, the quality of the global battery–vehicle coupled model is assessed according to the following two parameters:

$$\text{global distance traveled } = \sum_{k=1}^{n} v_k \cdot Ts \tag{24}$$

$$\text{total energy delivered} = \sum_{k=1}^{n} V_k \cdot I_k \cdot Ts \tag{25}$$

where v_k is the vehicle speed, T_s is sampling time or test time and equal to 0.1 s, V_k is battery voltage, I_k is battery current and k is the time index on data acquisition.

3.1. Battery Model

The battery pack model was tested by comparing the *simulated Voltage* and the correlated *Simulated Power* with the corresponding experimental values. The *Experimental Current* was retained input as shown in Figure 11. In the current analysis, the power signal has been considered in order to evaluate the effective behavior of the battery pack model in order to investigate the error propagated by sequential model chain.

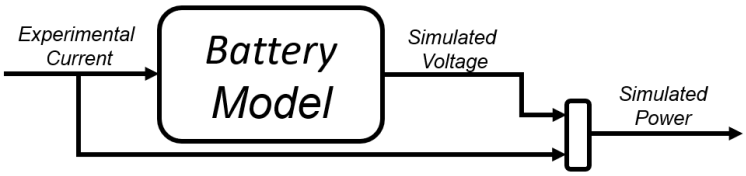

Figure 11. Battery model I/O scheme.

The discussed model implements an ECM for each cell. Each single Li-ion cell was modeled with the same parameters values, which were evaluated in the identification process. As is well-known in real-world applications, Li-ion cells inside a battery pack are slightly different from each other due to tolerances in the manufacturing process and temperature gradients. Consequently, cells may have different behaviors during working phases, and this motivates the need for a suitable BMS for battery state control. However, the hypothesis of similarity between the cells can be considered admissible [28,29] in this case given the relatively small impact on the two-wheeler range prediction.

As mentioned before, the cell parameters are identified over experimental data and valuable until SOC decreases down to 30% of the total available charge. The initial BMS limitation explained in the Methods section does not allow us to exploit the entire operating domain of the battery. However, the methodology can be extended to the value of SOC equal to 0% once more experimental tests to achieve complete discharge are carried out.

The model performance can be evaluated by comparing the model output and the experimental data regarding the voltage signal. As a result, after the calibration phase, the simulated voltage is plotted against the target voltage over time, as shown in Figure 12.

As shown in the figure, the relative residual error remains reasonably under 1% in absolute value for most of the simulated voltage points, while only a few 4% peaks are reached during transient discharging cycles. Moreover, Figure 12 contains the regression results in terms of fitted points. As is evident in the figure, the regression line described by the equation displayed exhibits fairly good superimposition with the bisector. Table 5 reports the *RMSE* and determination coefficient for the voltage estimated by the battery model developed.

Table 5. Battery Parameter Identification Voltage Metrics.

Test #	*RMSE* (V)	R^2
1	0.383	0.993

As Table 5 points out, the tuned battery parameters allow us to limit the *RMSE* with experimental data below 0.38 V. Moreover, the acceptable prediction capabilities have been demonstrated by the value of the R-squared-based metric being 99.3%.

In order to evaluate the range and performance of the two-wheeler, the electrical power delivered by the battery is provided as input to the vehicle model. Hence, the same analysis is carried out in order to estimate the residual error introduced by the battery modeling and propagated through the global model. Estimation results computed over the battery power can be observed in Figure 13.

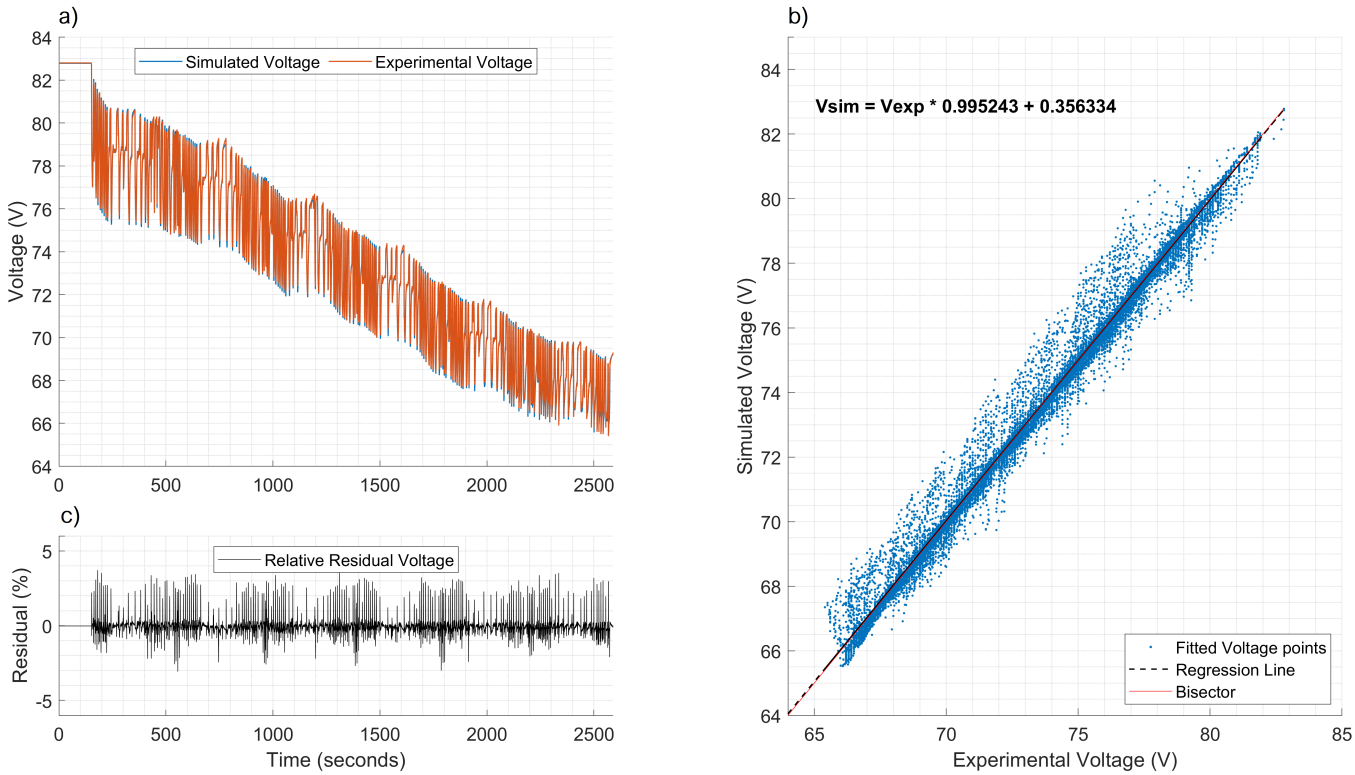

Figure 12. Test #1.1: regression process results for estimation of model voltage. (**a**) The simulated voltage and experimental voltage on real driving mission and (**c**) residual error of estimation. (**b**) Regression process results in terms of fitting equation and bisector comparison.

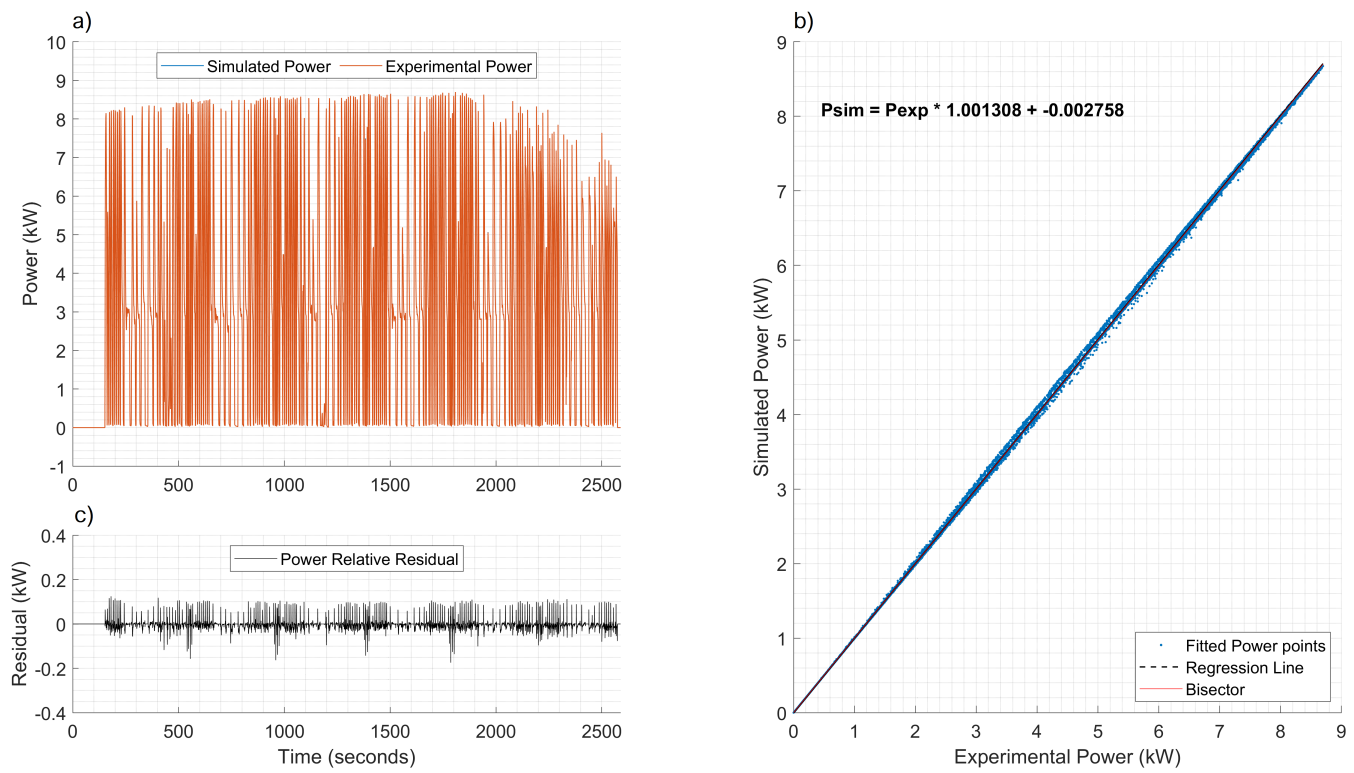

Figure 13. Test #1.1: Regression process results for estimation of model power. (**a**) The simulated and experimental power on real driving mission and (**c**) residual error of estimation. (**b**) Regression process results in terms of fitting equation and bisector comparison.

As we can see, the simulated power residual error remains in a narrow range between 0.1 kW and −0.1 kW. Also in this case, the residual error for most of the time points is significantly lower than 0.02 kW. Again, the consistency in the estimation results is highlighted by the appropriateness of the fitting process, as displayed in the right-hand sub-figure in Figure 13. The quality of the estimation is further confirmed by the statistical metric parameters computed and summarized in Table 6.

Table 6. Battery Parameter Identification Power and Energy Metrics.

Test #	*RMSE* (kW)	R^2	Experimental Energy Delivered (Wh)	Simulation Energy Delivered (Wh)	Relative Error Energy (%)
1	0.022	0.999	2409.3	2407.9	0.058

The error introduced by the battery model is low and acceptable so that negligible negative effects of error propagation can be observed. More details are shown in the results section concerning the global models. These results are confirmed by performing similar analyses on different datasets with respect to those used for the parameter identification in the calibration phase. The model testing is reported below in Tables 7 and 8 showing the same evaluation metrics.

Table 7. Battery Testing Voltage Metrics.

Test #	*RMSE* (V)	R^2
3.2	0.344	0.984
4.2	0.75	0.983
6.1	0.393	0.960
6.2	0.568	0.989
6.3	0.727	0.984
6.4	0.815	0.987
7	0.181	0.981

Table 8. Battery Testing Power and Energy Metrics.

Test #	*RMSE* (kW)	R^2	Experimental Energy Delivered (Wh)	Simulation Energy Delivered (Wh)	Error Energy (%)
3.2	0.035	0.999	158.8	157.9	0.527
4.2	0.076	0.999	158.6	161.5	1.852
6.1	0.006	0.999	54.5	54.9	0.573
6.2	0.022	0.999	114.8	115.9	0.980
6.3	0.051	0.999	190.7	193.2	1.300
6.4	0.079	0.999	308.7	312.9	1.382
7	0.007	0.999	86.3	86.5	0.182

As shown in Tables 7 and 8, the battery model achieves remarkable results in terms of battery voltage and electrical power. As far the electrical battery power is concerned, the high quality of the prediction capabilities have been demonstrated by values of R-squared being higher than 99% for each real-world driving mission in the performed tests. Again, the consistency in the prediction of the total energy delivered over on-road experimental tracks is highlighted by the percentage error remaining lower than 2%.

Some limitations occur in the model. First of all, the dependence of battery parameters on temperature is not taken into account due to the unavailability of experimental measurements. Therefore, in the next activities, new experimental tests will be performed

while also measuring the temperature of relevant powertrain components. It could be also interesting to take into account other environmental conditions, such as the ambient humidity for example, in order to evaluate the increase in accuracy in relation to a growing model complexity.

3.2. Vehicle Model

As shown in the Methods section, the electric scooter is modeled following a longitudinal dynamic approach, as shown in Equation (18). The test procedure was performed in accordance with Figure 14 showing the simplified vehicle scheme. The experimental battery power acquired during tests is the model input, and the predicted vehicle speed is the model output. The vehicle speed simulation is compared with experimental on-road data.

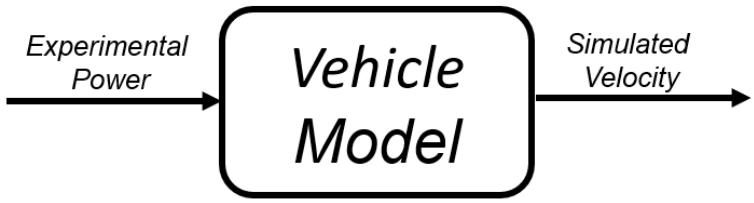

Figure 14. Vehicle model input/output scheme.

As mentioned earlier, the road's load-resistive power can be evaluated based on the coastdown test results. The fitting process allows us to identify the coefficients of polynomial Equation (16), which models the resistive phenomena included in Equation (15). The resulting values of the coefficients are hereafter reported in Table 9, while the trend of the resistive power as a function of vehicle velocity is shown in Figure 15.

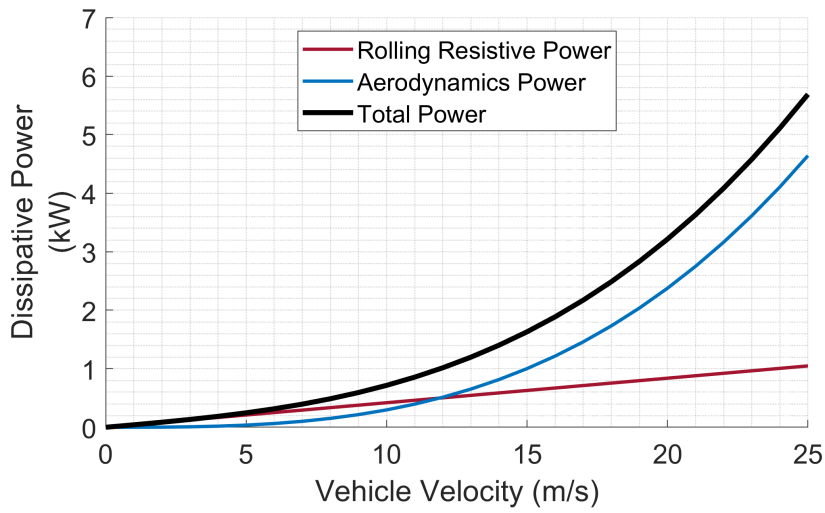

Figure 15. Road load power terms acting on vehicle body as a velocity-dependent function.

Table 9. Coastdown coefficients values for longitudinal dynamic vehicle modeling. *A*, *B* and *C* are the coefficients for describing the resistive forces depending on the vehicle speed.

Parameter	Value	U.d.m.
A	41.8	N
B	0	$\mathrm{N} \cdot \frac{\mathrm{s}}{\mathrm{m}}$
C	0.3	$\mathrm{N} \cdot \frac{\mathrm{s}^2}{\mathrm{m}^2}$

The two contributions of the road load power are the rolling and aerodynamic phenomena. As can be observed in Figure 15, the rolling term is predominant at low vehicle

speed, while at higher speed values, the aerodynamic forces are quite totally prevailing, consistent with well-known literature.

Once the vehicle road load is performed, the equivalent inertia of rotating components m_r and the global battery-to-road efficiency η_{b2r} were obtained following a cost-function minimization problem. The resulting numerical values can be found in Table 10.

Table 10. Vehicle dynamic model coefficients: m is the sum of the vehicle and driver masses, m_r is the value of the equivalent inertia of the rotating components and η_{b2r} is the overall battery-to-road efficiency, including the electric motors and transmission losses.

Name	Value	U.d.m.
m	184	kg
m_r	16	kg
η_{b2r}	0.75	-

Hence, considering Equation (17) and knowing the vehicle mass m and the frontal area A_f, the vehicle aerodynamic drag coefficient C_x and the tires' rolling resistance f have been accurately computed and shown in the Table 11.

Table 11. Aerodynamic and rolling resistance coefficient values of two-wheeler road load model.

Aerodynamic drag coefficient	C_x	0.81	-
Rolling resistance coefficient	f	11.62	$\frac{\text{kg}}{\text{t}}$

The portion of the literature reviewed by the authors lacks exhaustive experimental results in terms of the dragging and rolling coefficients of electric scooters. However, a study close to this has shown reasonably comparable values for the experimentally calibrated coefficients [42]. In order to evaluate the vehicle model performance, the procedure exploited for the battery was applied as well by comparing the model output with the relative experimental data. The vehicle speed predicted by the numerical model over the real-world driving mission was considered, and the residual error was assessed. As previously mentioned, braking was not modeled since it was not achievable by the prototype two-wheeler. Therefore, the braking torque was derived directly from experimental data in terms of speed and acceleration in order to ensure compliance with the overall energy balance over the entire driving mission. As it can be seen in Figure 16, the absolute error is generally lower than 2 m/s. However, some discrepancies between prediction and experimental data are observed. First, the braking phases estimation does not fit the measured data accurately in some braking events. Moreover, the road slope has not been taken into account in the model due to the absence of suitable acquisition sensors. Despite tests being developed on mainly flat roads, slight changes in the road slope were unavoidable. Finally, a finer assessment of the battery-to-road efficiency can be addressed in order to accurately predict the behavior of powertrain components. In conclusion, despite these simplifications, the model produces good results, and it is suitable for the purpose of the activity. The effectiveness of the total distance prediction provided by the numerical model is confirmed by the experimental results in the datasets exploited for both the parameter calibration and the testing task. Other than the training dataset shown in Figure 16, the prediction accuracy is illustrated in Figure 17.

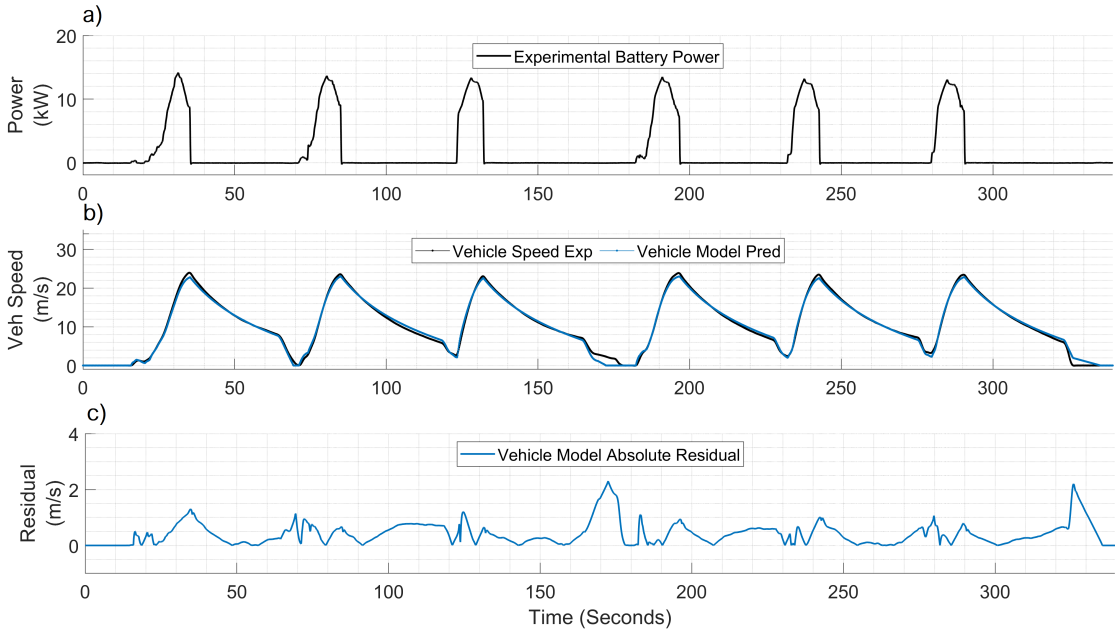

Figure 16. Test #4.1. Vehicle model performance: (**a**) battery power delivered, (**b**) predicted and measured velocity and (**c**) residual of the estimation.

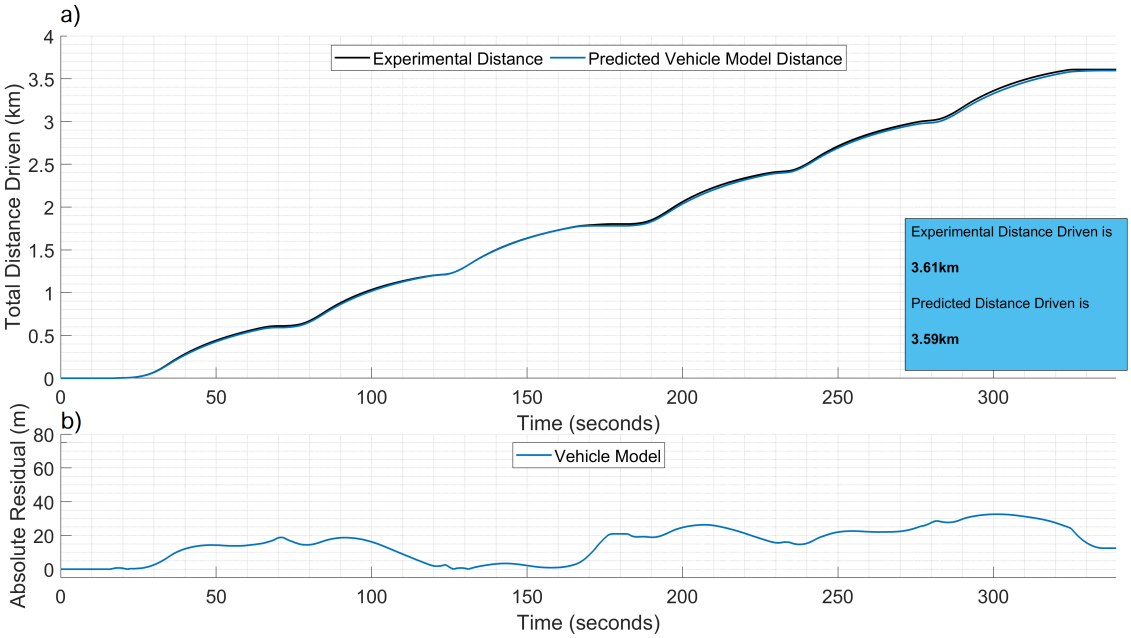

Figure 17. Test #4.1. Electric range prediction: (**a**) total distance traveled and (**b**) instantaneous absolute residual.

As it can be observed, the spatial distance predicted by the developed numerical model exhibits a fairly good accuracy with the experimental data collected. The instantaneous absolute error tends to remain acceptable, obtaining a relative error of about 0.55% at maximum for the distance driven.

Finally, the vehicle model prediction performance is evaluated over different cycles in real-world driving conditions and listed in Tables 12 and 13.

Despite being simple, the vehicle model can estimate the distance traveled by the electric two-wheeler over on-road experimental tests quite well. The electric range could therefore be accurately estimated thanks to the developed numerical model.

Table 12. Prediction metrics of vehicle model performance over parameter identification datasets.

Test #	*RMSE* (m/s)	R^2	Total Distance Traveled Experimental (km)	Total Distance Traveled Model (km)	Error Distance (%)
2.1	0.631	0.990	4.100	4.035	1.578
3.1	0.750	0.986	3.006	3.014	0.272
4.1	0.577	0.994	3.607	3.594	0.346
5.1	0.846	0.933	1.200	1.021	15.009
5.2	0.923	0.984	1.334	1.210	9.272
5.3	0.942	0.976	3.730	3.607	3.294
5.4	1.13	0.977	4.236	4.252	0.381

Table 13. Prediction metrics of vehicle model performance over testing datasets.

Test #	*RMSE* (m/s)	R^2	Total Distance Traveled Experimental (km)	Total Distance Traveled Model (km)	Error Distance (%)
3.2	0.914	0.978	3.13	3.12	0.496
4.2	0.503	0.996	3.60	3.61	0.334
6.1	0.507	0.974	1.95	1.86	4.90
6.2	0.638	0.987	2.98	2.85	4.41
6.3	0.908	0.982	3.48	3.42	1.89
6.4	0.788	0.991	4.67	4.62	0.93
7	1.171	0.973	1.59	1.53	3.32

3.3. Global Model

Finally, the global model assessment and validation are carried out connecting the battery and the dynamic vehicle model as a single sequential model chain. Looking at Figure 18, the global model was tested by exploiting the experimental current as a general input and comparing the simulated velocity with the experimental measured data.

Figure 18. Global model I/O scheme.

As detailed in the previous sections, the performance capabilities are investigated over different on-road driving missions. For this purpose, test 6.4 is targeted as the testing procedure for showing prediction results. As shown in Figure 19, satisfactory battery performance prediction is achieved in terms of battery pack voltage and power residual error with respect to the experimental measurements. As it can be analyzed from the voltage absolute residual error, only few 2 V peaks were reached. This is consistent with results shown in Figure 12 in the battery model section. Concerning the battery pack power output, the highest peaks of residual error are detected over the most severe transient conditions of the cycle which relate to battery pack current peaks and biggest residual error over voltage prediction. In the transient cycle tracks, the voltage prediction gap may relate to slight variations in the environmental temperature during the experimental test day. Therefore, the temperature issue can be addressed when an additional testing procedure will be performed in order to analyze the dependence of battery parameters on the temperature.

Finally, the spatial distance prediction capability of the global model has been investigated. Figure 20 shows the estimation of vehicle speed over the real-world driving mission by comparing the global model with the single vehicle model and experimental data.

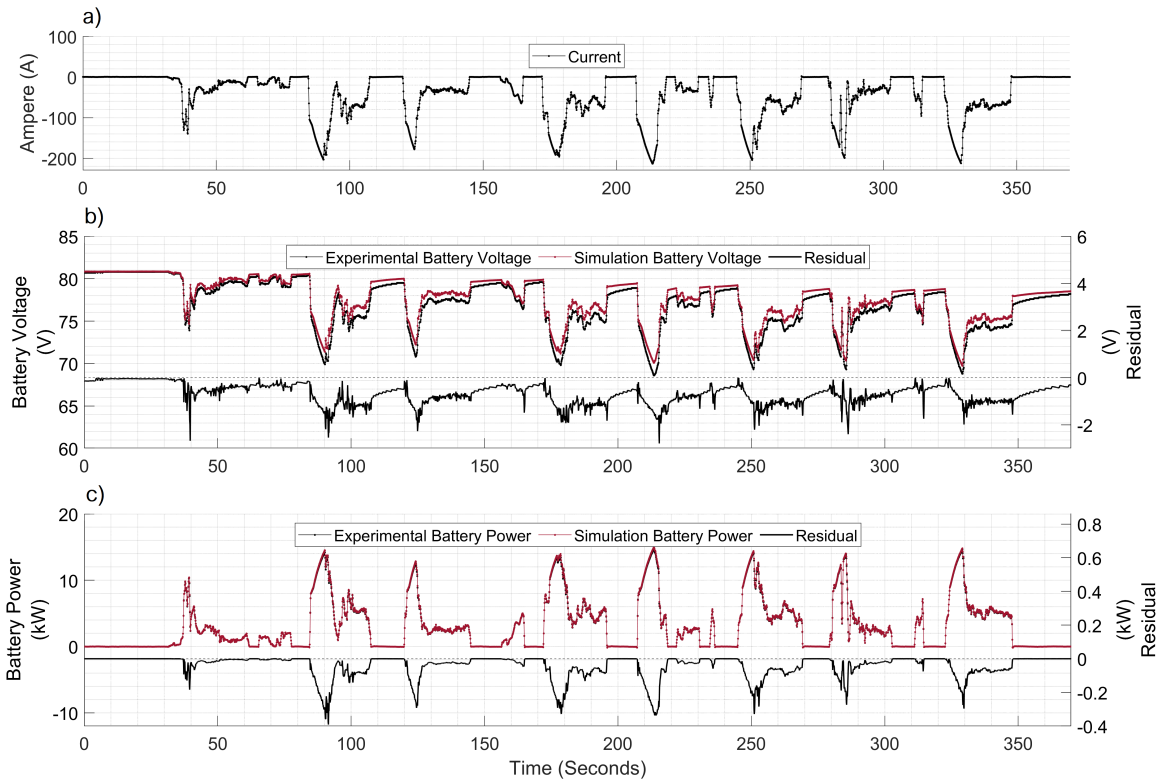

Figure 19. Test #6.4: (**a**) battery pack electrical current (A) as global model input, (**b**) battery pack voltage and (**c**) total battery pack power.

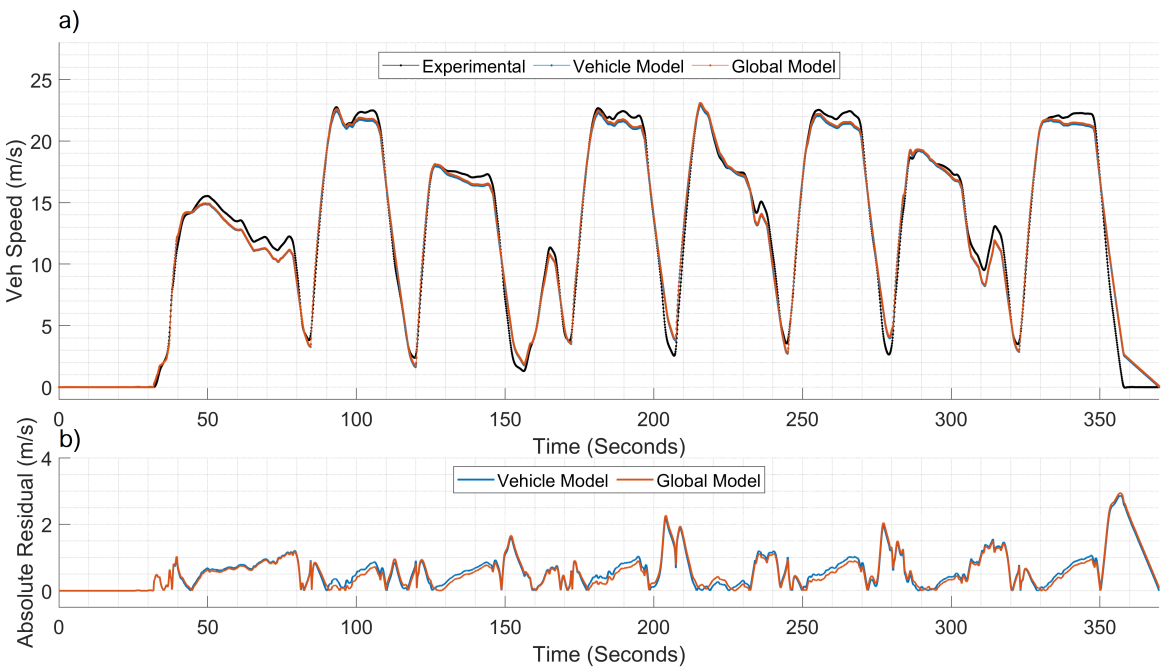

Figure 20. Test #6.4. Two-wheeler performance prediction: (**a**) the vehicle speed (m/s) of the global model compared to that of the single vehicle model and experimental data, (**b**) absolute residual error of global and vehicle models.

The global model evaluation results are shown in Figure 21.

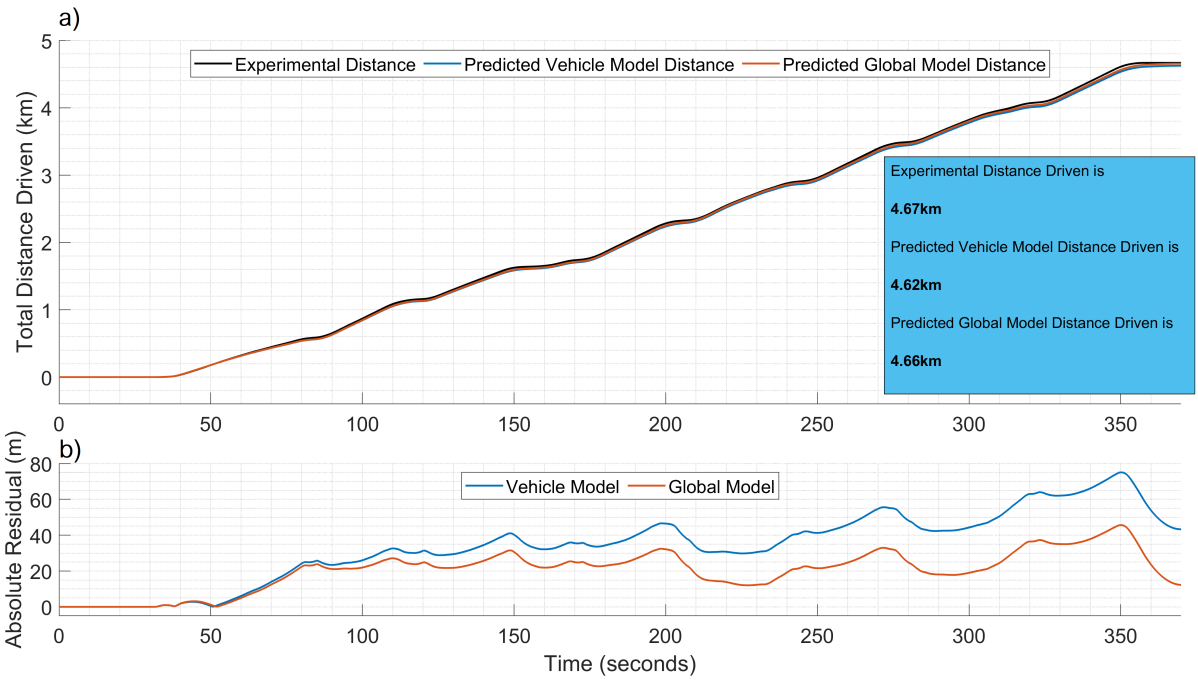

Figure 21. Test #6.4. (**a**) Total distance traveled by the two-wheeler expressed as electric range is estimated by the global model and compared with that of single vehicle model and experimental data. (**b**) Absolute residual error is plotted over the test time.

The total distance traveled by the vehicle along the mission is computed and the spatial distance is predicted, showing a relatively low instantaneous error. The overall results evaluated over the on-road, mission-based testing dataset are reported in Table 14.

Table 14. Prediction metrics of global model performance over testing datasets.

Test #	*RMSE* (m/s)	R^2	Total Distance Traveled Experimental (km)	Total Distance Traveled Model (km)	Error Distance (%)
3.2	0.917	0.978	3.13	3.11	0.763
4.2	0.503	0.996	3.60	3.64	1.106
6.1	0.492	0.975	1.95	1.87	4.539
6.2	0.610	0.987	2.98	2.87	3.855
6.3	0.892	0.982	3.48	3.44	1.209
6.4	0.777	0.991	4.67	4.66	0.263
7	1.169	0.973	1.59	1.53	3.225

From the comparison of Tables 13 and 14 concerning the testing datasets, the error in the total distance estimation as computed by the global model may be lower compared with the one attained by the single vehicle model. The single vehicle model is observed underestimating the total distance traveled by the vehicle. This may be due to the constant value of the global efficiency parameter η_{b2r}. This implies that the overall driveline losses are not dependent on the vehicle operating conditions. On the other hand, the battery model slightly overestimates the battery pack's electrical power. As a result, the two estimation errors tend to compensate for each other. Since the aim of the developed tool is range prediction, an underestimation error is preferred with respect to an overestimation one.

4. Conclusions

This study presented a detailed modeling approach to predict the performance of electric two-wheelers. A battery equivalent circuit model is coupled with an electric vehicle dynamic model into a global model to evaluate the prediction capabilities over real-world driving conditions. The global model parameters are calibrated over on-road experimental measurements. The developed model takes the battery pack electrical current as input and predicts the vehicle speed. Overall, the developed model has shown great capabilities for two-wheeler range estimation when real-world driving conditions are investigated. Moreover, the expected prediction results are consistent.

In future work, the achievement of increasing the prediction accuracy will be addressed, and the model's reliability over a larger operating domain of electrical components will be improved. At the very beginning, experimental tests must be carried out to account for temperature-varying LIB behavior. Hence, the cell model parameters will depend on thermal effects. In the same context, full discharge tests will be performed investigating the battery pack performance at very low SOC levels reaching 0%. Since the BMS should manage battery states, the SOC parameter has a key role in ensuring the acceptable lifetime of the battery pack. Hence, powerful algorithms for SOC real-time estimation can be implemented. Moreover, different battery pack configurations and chemistry will be analyzed in order to optimize the battery architecture and investigate aging phenomena.

The results of the developed and assessed numerical model suggest that the predictor tool can be embedded in BMS-integrated systems in order to develop different battery pack management strategies. Indeed, thanks to the developed vehicle model, the control logic for optimal Li-ion batteries management can be implemented afterwards in Software-in-the-Loop and Hardware-In-The-Loop environments.

Author Contributions: Conceptualization, A.F. and T.A.G.; methodology, A.F. and T.A.G.; software, A.F. and T.A.G.; validation, A.F. and T.A.G.; formal analysis, A.F. and T.A.G.; investigation, A.F. and T.A.G.; resources, A.F. and T.A.G.; data curation, A.F. and T.A.G.; writing—original draft preparation, A.F. and T.A.G.; writing—review and editing, A.F., T.A.G., D.M., P.G.A. and G.P.; visualization, A.F. and T.A.G.; supervision, D.M., P.G.A. and G.P.; project administration, D.M. and G.P.; All authors have read and agreed to the published version of the manuscript.

Funding: This research received no external funding.

Institutional Review Board Statement: Not applicable.

Informed Consent Statement: Not applicable.

Acknowledgments: We would like to thank the Danisi Engineering company for efforts spent on technical support and conducting the experimental on-road tests.

Conflicts of Interest: The authors declare no conflict of interest.

Nomenclature

LUT	Look-Up Table
BMS	Battery Management System
EV	Electric Vehicle
LIB	Lithium-Ion Battery
RC	Resistor Capacitor
EESS	Electrical Energy Storage System
ICE	Internal Combustion Engine
ECM	Equivalent Circuit Model
ECU	Electronic Control Unit
NLS	Non-Linear Square

V	Voltage
I	Current
SOC	State-of-Charge
SOH	State-of-Health
OCV	Open Circuit Voltage
R	Resistor
C	Capacitor
$RMSE$	Root Mean Square Error
R^2	Coefficient of determination
T_s	Sampling time
Q_{CELL}	Cell Capacity
m_{tot}	Total equivalent vehicle mass
a	Acceleration
v	Velocity
P_{mot}	Drive power
P_{diss}	Dissipative power
J_{motor}	Motor Inertia
θ	Motor rotational velocity
τ	Speed ratio between motor and driven wheel
m_r	Equivalent mass
η_{b2r}	Battery-to-road efficiency
F_{diss}	Dissipative Force
ρ_{air}	Air density
A_f	Frontal vehicle area
C_x	Drag coefficient
f	Rolling resistance coefficient

References

1. EVvolumes. The Electric Vehicle World Sales Database. Available online: https://www.ev-volumes.com/ (accessed on 26 January 2022).
2. Catenacci, M.; Verdolini, E.; Bosetti, V.; Fiorese, G. Going electric: Expert survey on the future of battery technologies for electric vehicles. *Energy Policy* **2013**, *61*, 403–413. [CrossRef]
3. Electric Vehicle Database. Available online: https://ev-database.org/cheatsheet/range-electric-car (accessed on 27 January 2022).
4. Masoud, M.; Elhenawy, M.; Almannaa, M.H.; Liu, S.Q.; Glaser, S.; Rakotonirainy, A. Optimal Assignment of e-scooter to Chargers. In Proceedings of the 2019 IEEE Intelligent Transportation Systems Conference, Auckland, New Zealand, 27–30 October 2019.
5. Kaneko, K.; Omori, H.; Kimura, N.; Morizane, T.; Nakaoka, M. A novel type of EDLC electric motor driven scooter with pulse super-rapied charger. In Proceedings of the 2015 International Conference on Electrical Drives and Power Electronics, Tatranska Lomnica, Slovakia, 21–23 September 2015.
6. Hwang Y.-L.; Cheng J.-K. The dynamic behavior and modal analysis of electric scooter. *J. Vibroeng.* **2014**, *16*, 2297–2304.
7. Locorotondo, E.; Pugi, L.; Berzi, L.; Pierini, M.; Lutzemberger, G. Online Identification of Thevenin equivalent circuit model parameters and estimation State of Charge of Lithium-Ion batteries. In Proceedings of the 2018 IEEE International Conference on Environment and Electrical Engineering and 2018 IEEE Industrial and Commercial Power Systems Europe (EEEIC/I&CPS Europe), Palermo, Italy, 12–15 June 2018; ISBN 978-1-5386-5186-5.
8. Marijn, R.; Jongerden, M.J. (University of Twente, Enschede, Overijssel, The Netherlands); Boudewijn, R.; Haverkort, H. (University of Twente, Enschede, Overijssel, The Netherlands). Personal communication, 2012.
9. Chen, M.; Rincon-Mora, G. Accurate electrical battery model capable of predicting runtime and IV performance. *IEEE Trans. Energy Convers.* **2006**, *21*, 504–511. [CrossRef]
10. Andre, D.; Meiler, M.; Steiner, K.; Walz, H.; Soczka-Guth, T.; Sauer, D.U. Characterization of high-power lithium-ion batteries by electrochemical impedance spectroscopy. II: Modelling. *J. Power Sources* **2011**, *196*, 5349–5356. [CrossRef]
11. Gao, L.; Liu, S.; Dougal, R. Dynamic lithium-ion battery model for system simulation. *IEEE Trans. Compon. Packag. Technol.* **2002**, *25*, 495–505.
12. Ángel Porras-Hermoso, A.P.-H.; Borja Cobo-Lopez, B.C.-L.; Santiago Pindado, S.P.; Javier Cubas, J.C. Analytical models for Li-ion batteries developed at the IDR/UPM Institute. In Proceedings of the 8th European Conference for Aeronautics and Space Sciences (EUCASS), Pza. del Cardenal Cisneros 3, Madrid, Spain, 1–4 June 2019. [CrossRef]
13. Klein, R.; Chaturvedi, N.A.; Christensen, J.; Ahmed, J.; Findeisen, R.; Kojic, A. Electrochemical Model Based Observer Design for a Lithium-Ion Battery. *IEEE Trans. Control Syst. Technol.* **2013**, *21*, 289–301. [CrossRef]
14. Smith, K.; Rahn, C.; Wang, C.-Y. Model-based electrochemical estimation and constraint management for pulse operation of lithium ion batteries. *IEEE Trans. Control Syst. Technol.* **2010**, *18*, 654–663. [CrossRef]

15. Tamilselvi, S.; Gunasundari, S.; Karuppiah, N.; Razak RK, A.; Madhusudan, S.; Nagarajan, V.M.; Sathish, T.; Shamim, M.Z.M.; Saleel, C.A.; Afzal, A. A Review on Battery Modelling Techniques. *Sustainability* **2021**, *13*, 10042. [CrossRef]
16. Bruen, T.; Marco, J.; Gama, M. Model Based Design of Balancing Systems for Electric Vehicle Battery Packs. *Int. Fed. Autom. Control* **2015**, *48*, 395–402. [CrossRef]
17. Ahmad, A.; Pesaran, P.A. Battery Thermal Management in EVs and HEVs: Issues and Solutions. In Proceedings of the Advanced Automotive Battery Conference, Las Vegas, NV, USA, 6–8 February 2001.
18. Janarthanam, S.; Paramasivam, S.; Maguire, P.; Gebbie, J.; Hughes, D. HEV Battery Pack Thermal Management Design and Packaging Solutions. *SAE Int. J. Engines* **2017**, *10*, 785–789. [CrossRef]
19. Yang, Z.; Patil, D.; Fahimi, B. Electrothermal Modeling of Lithium-Ion Batteries for Electric Vehicles. *IEEE Trans. Veh. Technol.* **2019**, *68*, 170-179. [CrossRef]
20. Specification of Product. Available online: https://batteryservice.bg/wp-content/uploads/2018/12/INR21700-50E.pdf (accessed on 18 February 2022).
21. Mathworks. Available online: https://it.mathworks.com/products/sysid.html (accessed on 28 January 2022).
22. Rajanna, B.V.; Kumar, M.K. Comparison of one and two time constant models for lithium ion battery. *Int. J. Electr. Comput. Eng.* **2020**, *10*, 670–680. [CrossRef]
23. Lv, J.; Jiang, B.; Wang, X.; Liu, Y.; Fu, Y. Estimation of the State of Charge of Lithium Batteries Based on Adaptive Unscented Kalman Filter Algorithm. *Electronics* **2020**,*9*, 1425. [CrossRef]
24. Jackey, R.; Saginaw, M.; Sanghvi, P.; Gazzarri, J.; Huria, T.; Ceraolo, M. Battery Model Parameter Estimation Using a Layered Technique: An Example Using a Lithium Iron Phosphate Cell. *SAE Tech. Pap.* **2013**,*1*, 1547.
25. García-Plaza, M.; Carrasco, J.; Peña-Asensio, A.; Alonso-Martínez, J.; Arnaltes Gómez, S. Hysteresis effect influence on electrochemical battery modeling. *Electric Power Syst. Res.* **2017**, *152*, 27–35. [CrossRef]
26. Jin, Y.; Zhao, W.; Li, Z.; Liu, B.; Liu, L. Modeling and Simulation of Lithium-ion Battery Considering the Effect of Charge-Discharge State. In Proceedings of the International Conference on Electronic Materials and Information Engineering, Xi'an, China, 9–11 April 2021.
27. Atalay, S.; Sheikh, M.; Mariani, A.; Merla, Y.; Bower, E.; Widanage, W.D. Theory of battery ageing in a lithium-ion battery: Capacity fade, nonlinear ageing and lifetime prediction. *J. Power Sources* **2020**, *478*, 7753. [CrossRef]
28. Yourey, W. Theoretical Impact of Manufacturing Tolerance on Lithium-Ion Electrode and Cell Physical Properties. *Batteries* **2020**, *6*, 23. [CrossRef]
29. Santhanagopalan, S.; White, R.E. Quantifying Cell-to-Cell Variations in Lithium Ion Batteries. *Int. J. Electrochem.* **2012**, *2012*, 395838. [CrossRef]
30. Van der Sluis, F.; Romers, L.; Van Spijk, G.; Hupkes, I. CVT, Promising Solutions for Electrification. *SAE Tech. Pap.* **2019**, *1*, 0359.
31. Swieczko-Zurek, B.; Jaskula, P.; Ejsmont, J.; Kedzierska, A.; Czajkowski, P. Rolling Resistance And Tire/Road Noise on Rubberized Asphalt Pavement in Poland. In Proceedings of the Rubberized Asphalt—Asphalt Rubber 2015 Conference, Las Vegas, NV, USA, 4–7 October 2015.
32. El-Sayegh, Z.; El-Gindy, M. Rolling resistance prediction of off-road tire using advanced simulation and analytical techniques. *SN Appl. Sci.* **2020**, *2*, 1620. [CrossRef]
33. Xiong, R.; Cao, J.; Yu, Q.; He, H.; Sun, F. Critical Review on the Battery State of Charge Estimation Methods for Electric Vehicles. *IEEE Access* **2018**, *6*, 1832–1843. [CrossRef]
34. Asep, N.; Estiko, R.; Danang, W.F.; Prapto, N. Battery state of charge estimation by using a combination of Coulomb Counting and dynamic model with adjusted gain. In Proceedings of the International Conference on Sustainable Energy Engineering and Application, Bandung, Indonesia, 5–7 October 2015.
35. Ion, P.; Dinu, C.; Gheorghe, C. Coast Down Test—Theoretical and Experimental Approach. In Proceedings of the International Automotive Congress, Brasov, Romania, 1 October 2010.
36. Carlson, R.; Lohse-Busch, H.; Diez, J.; Gibbs, J. The Measured Impact of Vehicle Mass on Road Load Forces and Energy Consumption for a BEV, HEV, and ICE Vehicle. *SAE Int. J. Altern. Powertrains* **2013**, *2*,105–114. [CrossRef]
37. Estimate Model Parameter Values (GUI). Available online: https://it.mathworks.com/help/sldo/ug/estimate-model-parameter-values-gui.html (accessed on 9 February 2022).
38. Estimate Model Parameter Values (Code). Available online: https://it.mathworks.com/help/sldo/ug/estimate-model-parameter-values-code.html (accessed on 9 February 2022).
39. Equation Solving Algorithms. Available online: https://it.mathworks.com/help/optim/ug/equation-solving-algorithms.html (accessed on 17 January 2022).
40. Least-Squares (Model Fitting) Algorithms. Available online: https://it.mathworks.com/help/optim/ug/least-squares-model-fitting-algorithms.html (accessed on 17 January 2022).
41. Zhang, C.; Allafi, W.; Dinh, Q.; Ascencio, P.; Marco, J. Online estimation of battery equivalent circuit model parameters and state of charge using decoupled least squares technique. *Energy* **2018**, *142*, 678–688. [CrossRef]
42. Jorge, I.; Mesbahi, T.; Paul, T.; Samet, A. Study and simulation of an electric scooter based on a dynamic modelling approach. In Proceedings of the 2020 Fifteenth International Conference on Ecological Vehicles and Renewable Energies (EVER), Monte-Carlo, Monaco, 10–12 September 2022.